International Journal of Heat and Mass Transfer 90 (2015) 838–847

Contents lists available at ScienceDirect

International Journal of Heat and Mass Transfer

journal homepage: www.elsevier.com/locate/ijhmt

Pore-scale and volume-averaged numerical simulations of melting phase change heat transfer in finned metal foam

Shangsheng Feng [a,b], Meng Shi [c], Yifei Li [c], Tian Jian Lu [a,b,*]

[a] MOE Key Laboratory for Multifunctional Materials and Structures (LMMS), School of Aerospace, Xi'an Jiaotong University, Xi'an 710049, PR China
[b] State Key Laboratory of Mechanical Structure Strength and Vibration, School of Aerospace, Xi'an Jiaotong University, Xi'an 710049, PR China
[c] School of Energy and Power Engineering, Xi'an Jiaotong University, Xi'an 710049, PR China

ARTICLE INFO

Article history:
Received 1 March 2015
Received in revised form 30 June 2015
Accepted 30 June 2015
Available online 24 July 2015

Keywords:
Metal foam
Phase change material (PCM)
Pore-scale numerical simulation
Local thermal equilibrium

ABSTRACT

The melting process of phase change material (PCM) infiltrated in a finned metal foam was numerically investigated using two approaches: (a) pore-scale and (b) volume-averaged numerical simulations. The pore-scale simulation modeled the intricate geometry of the open-cell metal foam using sphere-centered tetrakaidecahedron and coupled the heat transfer in foam/fin solids with that in the PCM. The volume-averaged simulation used the Darcy–Brinkman–Forchheimer model to account for the motion of melt PCM as well as the one-temperature model based on local thermal equilibrium assumption. The volume-averaged simulation results were compared with the pore-scale simulation results which were used as the benchmark. Reasonable agreement between prediction results of the two approaches was observed. When using the volume-averaged method, the one-temperature model may be applicable without needing the more complicated two-temperature model. The thermal performance of the finned metal foam was compared with conventional plate-fin and metal foam structures, demonstrating its superiority as thermal conductivity enhancer of PCM.

1. Introduction

Upon solid–liquid phase transition, phase change materials (PCMs) have the capability of storing and releasing sizeable latent heat. PCMs have therefore been widely used in applications requiring thermal management and thermal energy storage. However, most PCMs suffer from low thermal conductivity, which either prolongs the energy charging/discharging periods under isothermal boundary condition or increases the surface temperature under isoflux boundary condition.

Porous media is a common technique used for enhancing the heat transfer rate of PCMs, e.g., by encapsulating PCMs in packed spheres to increase the heat transfer area [1–4], or by introducing conductive porous matrix such as metal foams into PCMs [5,6]. Upon extensive review of existing conductivity enhancers, Fernandes et al. [7] argued that metal foam is one of the most promising material for increasing the heat transfer rate of PCMs. Recently, it was found that the convective heat transfer of metal foam could be further improved by incorporating solid fins into the metal foam forming the "finned metal foam" [8–10]. The enhancement was attributed to the fact that the solid fins promote heat conduction to the foam matrix. At present, the performance of finned metal foam for increasing the heat transfer rate of PCMs has not been investigated in the open literature, this study aims to deal with this issue using both pore-scale and volume-averaged numerical methods.

Broadly speaking, to simulate thermal fluid flow in a porous medium, two methods can be employed: *microscopic* and *macroscopic* approach. In the *microscopic* approach, the intricate geometry of the porous medium is accounted for and the pore-scale thermal fluid flow is computed. In the *macroscopic* approach, pore-scale distribution is not the concern; alternatively, only the global thermal fluid flow in the domain is predicted by solving the volume-averaged governing equations. Based on local thermal equilibrium or non-equilibrium assumption, the volume-averaged method may employ either one- or two-temperature model as the energy equation. The one-temperature model utilizes an identical energy equation for the two phases of the porous medium; and the two-temperature model employs a separate energy equation for each the phase, with heat transfer between the two phases modeled using interstitial heat transfer coefficients which are determined empirically. In comparison, the pore-scale simulation considers the intricate foam geometry and couples the heat

* Corresponding author at: MOE Key Laboratory for Multifunctional Materials and Structures (LMMS), School of Aerospace, Xi'an Jiaotong University, Xi'an 710049, PR China.
E-mail address: tjlu@mail.xjtu.edu.cn (T.J. Lu).

http://dx.doi.org/10.1016/j.ijheatmasstransfer.2015.06.088
0017-9310/

Nomenclature

a	cell size of metal foam (mm)
c_p	heat capacity (J/kgK)
f_l	liquid fraction
k	thermal conductivity (W/mK)
L	latent heat (J/kg)
T	temperature (K)
T_m	melting temperature (K)
u	velocity (m/s)

Greek Symbols

ρ	density (kg/m^3)
β	thermal expansion coefficient (1/K)
μ	viscosity (N s/m^2)
ε	porosity

Subscripts

f	phase change material
s	aluminum

transfer between the foam matrix and the PCM, without needing the assumption of local thermal equilibrium and any empirical interstitial heat transfer coefficients for closure. However, the pore-scale simulation requires much more computational resources thus is typically applied only for computational domain containing limited foam cells.

Beckermann and Viskanta [11] based on the volume-averaged method presented one of the pioneering works to simulate solid/liquid phase change in porous media with natural convection in the melt region. Their prediction results with the one-temperature model agreed well with experimental results using gallium and glass beads as the PCM and the porous matrix. Harris et al. [12] developed a theoretical enthalpy model to study the phase-change process in porous medium with the two-temperature model. Mesalhy et al. [13] investigated melting phase change heat transfer in metal foams saturated with PCM inside an annular space using the two-temperature model. The interstitial heat transfer coefficient between the foam matrix and the PCM was estimated by analyzing quasi-steady heat conduction in two cylindrical layers, with liquid phase motion neglected. Krishnan et al. [14] numerically investigated the melting process of PCM embedded in a metal foam using the two-temperature model. They artificially changed the interstitial heat transfer coefficient to investigate the criterion for local thermal equilibrium. Their results showed that when the interstitial Nusselt number exceeds a certain value, the two-temperature model yields the same predictions as the one-temperature model. However, when the one-temperature model can replace the more complex two-temperature model is still unclear, since the actual interstitial heat transfer coefficients in practical systems are unknown. Tian and Zhao [15] adopted the two-temperature model to simulate the thermal performance of PCM (paraffin) embedded in a metal foam heated from the bottom and found that global natural convection of liquid PCM is not strong enough to produce dominant influence on heat transfer. Li et al. [16] simulated the same problem but heating at the side boundary, they found significant natural convection of liquid PCM. Tian and Zhao [15] and Li [16] both determined the interstitial heat transfer coefficient between the foam matrix and the liquid PCM using the Nusselt number correlations for flow across stagger cylinders, and assumed thermal insulation between the foam matrix and the solid PCM.

In contrast to the *macroscopic* approach, few studies [17–19] performed pore-scale simulation on phase change heat transfer in metal foams. Hu and Patnalk [17] modeled PCM in a micro-foam using pore-scale numerical simulation with natural convection of the liquid PCM ignored. Using pore-scale simulation, Sundarram and Li [18] investigated the effects of pore size and porosity of microcellular metal foam on phase change heat transfer. Their results indicated that the velocity of PCM movement during melting is insignificantly small (on the order of 10^{-8} m/s). Recently, Chen et al. [19] used a lattice Boltzmann model to study two-dimensional pore-scale melting of PCM in metal foam and obtained good agreement with experimental observations.

The above literature survey shows that most existing studies used the two-temperature model in volume averaged simulations, especially for metal foams [13–16]. Relative to the one-temperature model, the two-temperature model is physically more reasonable, it nevertheless requires interstitial heat transfer coefficients between the foam matrix and the PCM for closure which were determined quite differently in previous studies [13–16]. The uncertainties of the interstitial heat transfer coefficients may introduce model prediction errors. On the other hand, the one-temperature model does not need the interstitial heat transfer coefficients and it is easier to implement numerically. Is the one-temperature model applicable to simulate PCM in metal foam? This important question will be explored in this study.

A case study for melting of paraffin infiltrated in a finned metal foam was carried out to explore the local thermal equilibrium between metal foam and paraffin. To this end we used two simulation methods: the *pore-scale* and *volume-averaged* simulations. The *pore-scale* simulation results were used as benchmark to demonstrate whether the one-temperature model (in *volume-averaged* simulation) is applicable for paraffin infiltrated metal foam or not. Results obtained from the two simulation methods were compared with each other under two different conditions separately: with and without considering natural convection of liquid PCM inside the foam. Furthermore, the thermal performance of the finned metal foam was compared with those of the conventional plate-fin and metal foam structures as thermal conductivity enhancer of PCM.

2. Problem description

Fig. 1 depicts schematically the physical problem to be tackled in the study. The finned metal foam considered is consisted of solid fins and high porosity open-cell metal foam blocks, both made of pure aluminum (Al). Thermal contact resistance is not considered as metal foam blocks are assumed properly bonded to solid fins through sintering or high thermal conductivity adhesive. Docosane (paraffin wax with $C_{22}H_{46}$ composition) as the PCM is impregnated into the pore space of each foam block. The thickness (t) and height (H) of each fin are 1 mm and 30 mm, respectively, and the width (s) between two adjacent fins is 10 mm. The open-cell foam has a cell size of 5 mm and a porosity of 0.97 (predicted by Eq. (1)). Thus, between two adjacent fins, there are 2×6 foam cells along the width and height directions.

The bottom surface of the finned metal foam is heated with a constant temperature of T_w = 347 K, which is higher than the melting temperature of docosane T_m = 317 K. All other external surfaces of the finned metal foam are assumed adiabatic. Initial temperature (T_0) of the PCM and the finned metal foam is 300 K.

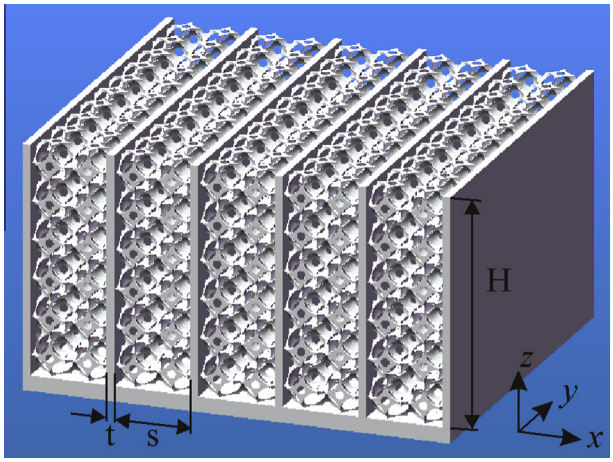

Fig. 1. Illustration of PCM embedded into finned metal foam.

Table 1
Thermo-physical parameters of PCM (docosane) and aluminum (Al).

	ρ (kg/m^3)	c_p (J/kg-K)	k (W/m-K)	L (kJ/kg)	T_m (K)	μ (kg/m-s)	β (1/K)
PCM	785	2890	0.4	260	317	2.63×10^{-2}–$6.87 \times 10^{-5}.T_f$	0.0011
Al	2719	871	202.4	N/A	N/A	N/A	N/A

Relevant thermo-physical parameters of the docosane and aluminum are shown in Table 1, where the viscosity and thermal expansion coefficient are extracted from Ref. [20] and the remaining parameters are taken from Ref. [17].

3. Model and methods

3.1. Pore-scale numerical simulation

The pore-scale numerical simulation requires reconstruction of the intricate foam geometry. In the present study, the cellular morphology of the aluminum foam was modeled with sphere-centered tetrakaidecahedron due to its similarity with the real aluminum foam having open cells as shown in Fig. 2(a). The creation process of the sphere-centered tetrakaidecahedron is illustrated in Fig. 2(b) [21]. A tetrakaidecahedron was first generated by cutting off the six corners of a regular octahedron. Then a sphere at the center of the tetrakaidecahedron was subtracted from it to obtain the tetrakaidecahedron with spherical pore. Upon packing the sphere-centered tetrakaidecahedron cells in three dimensional (3D) space, the network structure of the open-cell foam was obtained as depicted in Fig. 1.

Given that the foam geometry is modeled with the sphere-centered tetrakaidecahedron, the porosity of the metal foam can be calculated as:

$$\varepsilon = -\frac{\pi}{4}\left[8\left(\frac{D}{a}\right)^3 - 2(3+2\sqrt{3})\left(\frac{D}{a}\right)^2 + 2 + \sqrt{3}\right] \tag{1}$$

$$d = \sqrt{D^2 - \frac{a^2}{12}} \tag{2}$$

where a (characterizing the cell size) is the distance between two opposite quadrilateral faces of the tetrakaidecahedron, D is the diameter of the sphere, and d is the diameter of the circle on the hexagonal faces of the tetrakaidecahedron, as shown in Fig. 2(b).

Due to periodicity only a single fin-foam channel (referring to Fig. 1) was considered, further thanks to the symmetry of geometry only half of a fin-foam channel was included in the computation domain. Since there were many unit cells along the y-axis, the thermal fluid flow in different unit cells along the y-axis was assumed periodic, therefore only one unit cell along the y-axis was simulated to save the computational time. As a result, the final computational domain included half a fin and 1×6 foam cells, as shown in Fig. 3(a). Fig. 3(b) shows the mesh generated at the fin and foam region with that at the PCM region omitted for clarity.

The thermophysical properties of aluminum and PCM (listed in Table 1) were assumed to be constant over the range of temperature considered. Volume change of the PCM upon phase changing was ignored. The liquid PCM was assumed to be incompressible, Newtonian, and subject to the Boussinesq approximation. Based on the above assumptions, the governing equations for fluid-flow of the liquid PCM may be written as:

$$\nabla \cdot \vec{u} = 0 \tag{3}$$

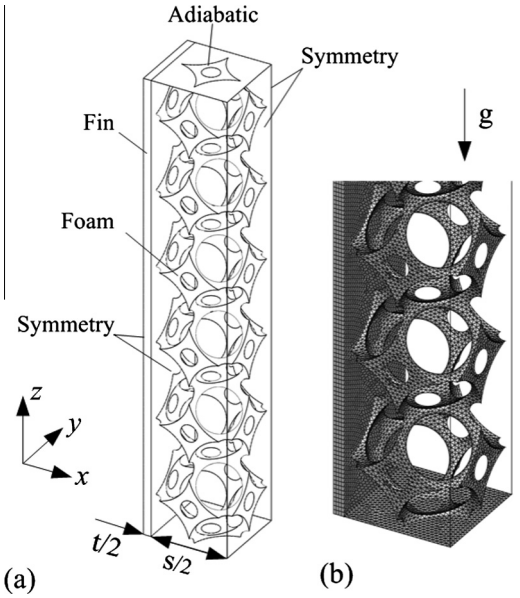

Fig. 3. Pore-scale numerical simulation: (a) computational domain; (b) meshing of fin and foam, with PCM zone grid points omitted for clarity.

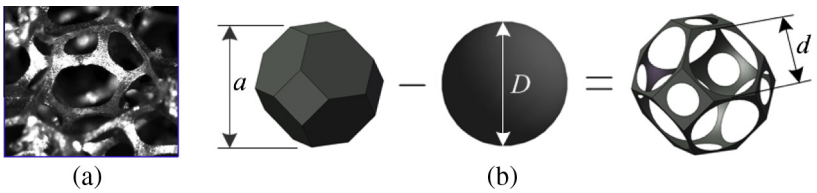

Fig. 2. Foam geometry: (a) SEM picture; (b) idealized unit cell.

$$\rho_f \frac{\partial \vec{u}}{\partial t} + \rho_f(\vec{u}\cdot\nabla)\vec{u} = -\nabla P + \mu_f \nabla^2 \vec{u} + \rho_f \vec{g}\,\beta(T_f - T_m) + A\vec{u} \tag{4}$$

The last term in Eq. (4) is an additional source to damp the velocity in solid PCM [22]:

$$A = \frac{C(1-f_l)^2}{S + f_l^3} \tag{5}$$

f_l is the liquid fraction, which has value 1 in the liquid PCM region, 0 in the solid PCM region, and 0–1 in the mushy region. C and S are arbitrary big and small values, set here as 10^5 and 10^{-3}, respectively [22].

Heat transfer in the (solid and liquid) PCM regions was described as:

$$\rho_f c_{pf} \frac{\partial T_f}{\partial t} + \rho_f c_{pf} \vec{u}\cdot\nabla T_f = \nabla\cdot(k_f \nabla T_f) - \rho_f L \frac{\partial f_l}{\partial t} \tag{6}$$

Liquid fraction in the last term of Eq. (6) was updated according to PCM temperature, as:

$$f_l = \begin{cases} 0 & T_f \leqslant T_{m1} \\ (T_f - T_{m1})/(T_{m2} - T_{m1}) & T_{m1} \leqslant T_f \leqslant T_{m2} \\ 1 & T_f \geqslant T_{m2} \end{cases} \tag{7}$$

For numerical stability, phase change was assumed to occur over a small but finite temperature range ($T_{m1} \sim T_{m2}$), with T_{m1} and T_{m2} set to be 0.1 °C lower and higher than the melting temperature respectively.

Heat transfer in the fin and foam matrix was governed by transient heat conduction equation, as:

$$\rho_s c_{ps} \frac{\partial T_s}{\partial t} = \nabla\cdot(k_s \nabla T_s) \tag{8}$$

Temperature and heat flux continuity were considered at the interface between PCM and fin/metal foam, as:

$$T_f = T_s, \quad k_f \frac{\partial T_f}{\partial n} = k_s \frac{\partial T_s}{\partial n} \tag{9}$$

3.2. Volume-averaged numerical simulation

In the volume-averaged simulation, the PCM infiltrated metal foam was treated as a homogeneous and continuous medium. Volume-averaged governing equations were used to describe flow and heat transfer in the PCM/foam composite and coupled with the heat conduction equation for the solid fin. Due to volume-averaging, the computational domain was reduced to a two dimensional (2D) one containing half of a fin-foam channel, as shown in Fig. 4. The foam in the computational domain was assumed to be isotropic. Note that this assumption may be questionable, given that there was only one foam cell in the x-direction within the computational domain. Actually, how many cells are enough to justify the assumption of foam isotropy remains an open question.

The effect of foam matrix on motion of liquid PCM was considered using the Darcy–Brinkman–Forchheimer model, as:

$$\nabla\cdot\langle\vec{u}\rangle = 0 \tag{10}$$

$$\frac{\rho_f}{\delta}\frac{\partial\langle\vec{u}\rangle}{\partial t} + \frac{\rho_f}{\delta^2}(\langle\vec{u}\rangle\cdot\nabla)\langle\vec{u}\rangle = -\nabla\langle P\rangle^f + \frac{\mu_f}{\delta}\nabla^2\langle\vec{u}\rangle - \left(\frac{\mu_f}{K} + \frac{\rho_f C_f}{\sqrt{K}}|\langle\vec{u}\rangle|\right)\langle\vec{u}\rangle + \rho_f\vec{g}\,\beta(\langle T_f\rangle - T_m) + A\langle\vec{u}\rangle \tag{11}$$

where K is the permeability, C_f is the form drag coefficient, and ε is the porosity of the metal foam; δ is the liquid fraction of PCM in the porous medium:

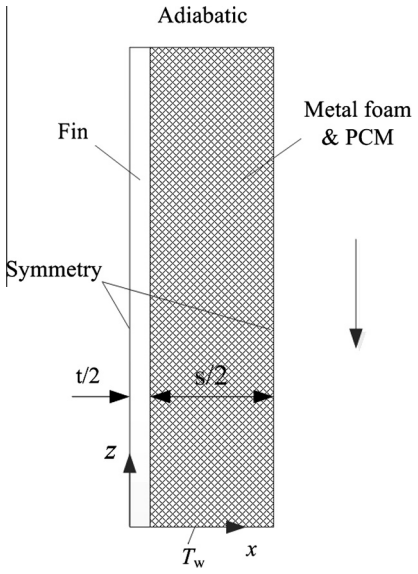

Fig. 4. Computational domain and boundary conditions in volume-averaged numerical simulation.

$$\delta = \varepsilon\cdot f_l \tag{12}$$

Based on the assumption of local thermal equilibrium, the one-temperature model was adopted to describe the heat transfer in the PCM/foam composite, as:

$$(\varepsilon\rho_f c_{pf} + (1-\varepsilon)\rho_s c_{ps})\frac{\partial\langle T_f\rangle}{\partial t} + \rho_f c_{pf}\langle\vec{u}\rangle\cdot\nabla\langle T_f\rangle = \nabla\cdot(k_{ef}\nabla\langle T_f\rangle) - \rho_f\varepsilon L\frac{\partial f_l}{\partial t} \tag{13}$$

where k_{ef} is the effective thermal conductivity of the PCM/foam composite. The validity of the one-temperature model will be discussed later.

Heat conduction in the solid fin was governed by Eq. (8). At the interface between the fin and the PCM/foam composite temperature and heat flux continuity was considered as:

$$\langle T_f\rangle = T_s, \quad k_{ef}\frac{\partial\langle T_f\rangle}{\partial n} = k_s\frac{\partial T_s}{\partial n} \tag{14}$$

In Eqs. (10)–(13), $\langle\phi\rangle$ denotes the extrinsic average of a quantity over a representative elementary volume (REV) of the porous medium, and $\langle\phi\rangle_f$ and $\langle\phi\rangle_s$ refer to the intrinsic averages over the fluid and solid part of the REV, respectively. The extrinsic and intrinsic averages of a generic transport variable are defined as:

$$\langle\phi\rangle = \varepsilon\langle\phi\rangle_f, \quad \langle\phi\rangle = (1-\varepsilon)\langle\phi\rangle_s \tag{15}$$

The permeability and the form drag coefficient appearing in Eq. (11) were determined using the models provided in Ref. [23], whereas the effective thermal conductivity appearing in Eq. (13) was evaluated using the model provided in Ref. [24], which are summarized below as:

$$\frac{K}{a^2} = 0.00073(1-\varepsilon)^{-0.224}\left[1.18\sqrt{\frac{(1-\varepsilon)}{3\pi}}\left(\frac{1}{1-e^{-((1-\varepsilon)/0.04)}}\right)\right]^{-1.11} \tag{16}$$

$$C_f = 0.00212(1-\varepsilon)^{-0.132}\left[1.18\sqrt{\frac{(1-\varepsilon)}{3\pi}}\left(\frac{1}{1-e^{-((1-\varepsilon)/0.04)}}\right)\right]^{-1.63} \tag{17}$$

$$k_{ef} = 0.35(\varepsilon k_f + (1-\varepsilon)k_s) + \frac{0.65}{\left(\frac{\varepsilon}{k_f} + \frac{1-\varepsilon}{k_s}\right)} \quad (18)$$

It should be mentioned that Eqs. (16)–(18) have been verified against pore-scale simulation results based on a body-centered-cubic (BCC) model [25], which is similar to the present sphere-centered tetrakaidecahedron model for open-cell metal foam.

3.3. Problem setup

CFD package ANSYS FLUENT 14.0 was used for pore-scale numerical simulation with double precision. The Second Order Upwind scheme was adopted for discretizing the convective terms in the governing equations. The SIMPLE method was employed for the pressure correction equation. The under-relaxation factors for the momentum, pressure correction, thermal energy, and liquid fraction were set separately as 0.5, 0.3, 0.7, and 0.6 to ensure convergence. The convergence criterion of absolute scaled residual for the momentum and energy equations was separately 10^{-5} and 10^{-8}. The time-step was set as $dt = 0.01$ s, which has been found small enough to obtain time-step independent results by comparing with the results obtained from $dt = 0.005$ s. Un-structured grids were generated in the fin, the foam matrix, and the pore space filled with PCM, as shown in Fig. 3(b). The mesh independency study was performed using two different grids (coarse grid with 290 k cells and fine grid with 570 k cells). It was established that the two grids yielded the same prediction results, as shown in Fig. 5.

For volume-averaged numerical simulation, the governing equations were solved using a Fortran code based on the finite-volume-method, which has been validated in several previous works [10,26,27]. A staggered grid system was employed, where the velocities were stored at the control-volume faces whilst all other variables were calculated at the grid points. The structured mesh of 36×60 grid points was found enough for obtaining mesh independency results. The SIMPLE algorithm was employed for the pressure correction equation. The discretized equations were solved by the line-by-line procedure which is a combination of the Tri-Diagonal-Matrix Algorithm (TDMA) and the Gauss–Seidel iteration technique of Patankar [28]. The time-step and convergence criterion were identical to those used in the pore-scale simulation.

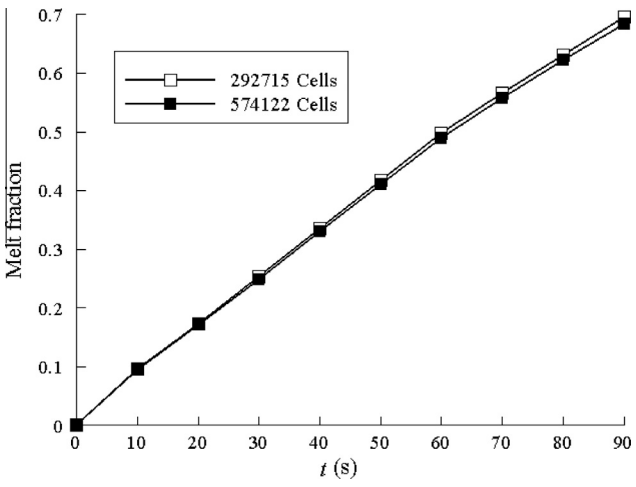

Fig. 5. Mesh independency study of the pore-scale numerical simulation.

4. Results and discussion

The pore-scale and volume-averaged simulation methods have been developed to explore melting process of PCM infiltrated in a finned metal foam. The solid–liquid phase, temperature, and velocity distributions obtained from the two methods are qualitatively compared in the Section 4.1.1. In Section 4.1.2 quantitative comparison of results obtained from the two methods is presented in terms of the melt fraction and surface heat flux. In Section 4.2, the thermal performance of the proposed finned metal foam is compared with the conventional plate-fin and metal foam structures as thermal conductivity enhancer of PCM.

4.1. Comparison of results predicted by the two simulation methods

4.1.1. Solid–liquid phase, temperature, and velocity distributions

Fig. 6(a) depicts the pattern of solid–liquid phase distributions (at melt fraction = 0.25) predicted by the volume-averaged method. The corresponding pore-scale simulation results are shown in Fig. 6(b) at five selected slices of $y/a = 0$, 1/8, 1/4, 3/8 and 1/2. In Fig. 6, the red and blue colors represent separately the liquid and solid PCM, and the gray stands for the fin and the foam matrix. Melting is initiated from the bottom heated surface and the vertical fin surface due to the relative high temperature at these surfaces, then the phase front propagates upward from the bottom surface and inward from the vertical fin. As a result, the phase front appears a "U" shape, as shown in Fig. 6(a) and (b) for half of the phase distributions. Overall, the two simulation methods predict qualitatively similar solid–liquid phase distribution behaviors. However, the volume-averaged simulation could only predict the overall phase distribution information such as the "U" shaped phase front due to the homogeneous treatment of the foam/PCM composite. In comparison, the pore-scale simulation is able to capture the local melting behavior, e.g., local melting of PCM around foam struts as marked by the hot spots in slices 2 and 3 of Fig. 6(b), and at the center of the first bottom unit some solid PCM is surrounded by liquid phase as shown in slices 4 and 5 of Fig. 6(b).

Figure 7(a) and (b) presents temperature distributions predicted by the volume-averaged and the pore-scale simulation methods respectively, again with melt fraction = 0.25. As shown in Fig. 7, the temperature distributions are consistent with the phase distributions presented in Fig. 6. For instance, the isothermal line corresponding to the melting temperature ($T_m = 317$ K) resembles the phase front. The PCM below the phase front (temperature < T_m) is in solid phase, and the PCM on top of the phase front (temperature > T_m) is in liquid phase. It was found that the temperature gradient in the liquid PCM is significantly higher than that in the solid PCM, especially near the phase front. The higher and lower temperature gradients in the liquid and solid PCM indicate that the majority of heat is transferred from the fin/foam and bottom surface to the liquid PCM, while very limited heat is absorbed by the solid PCM. The particularly high temperature gradient near the phase front further indicates that a large portion of heat becomes the latent heat of PCM during the melting process.

To complement the qualitative comparison between the two simulation methods, the flow field of melt PCM due to natural convection predicted by the two simulation methods are presented in Fig. 8 (a) and (b), respectively. In the finned metal foam, the presence of the solid fin causes the temperature of PCM near the fin higher than that at the channel center. Due to buoyancy the melt PCM with higher temperature nearby the fin surface rises upward along the fin, and the PCM at the channel center with lower

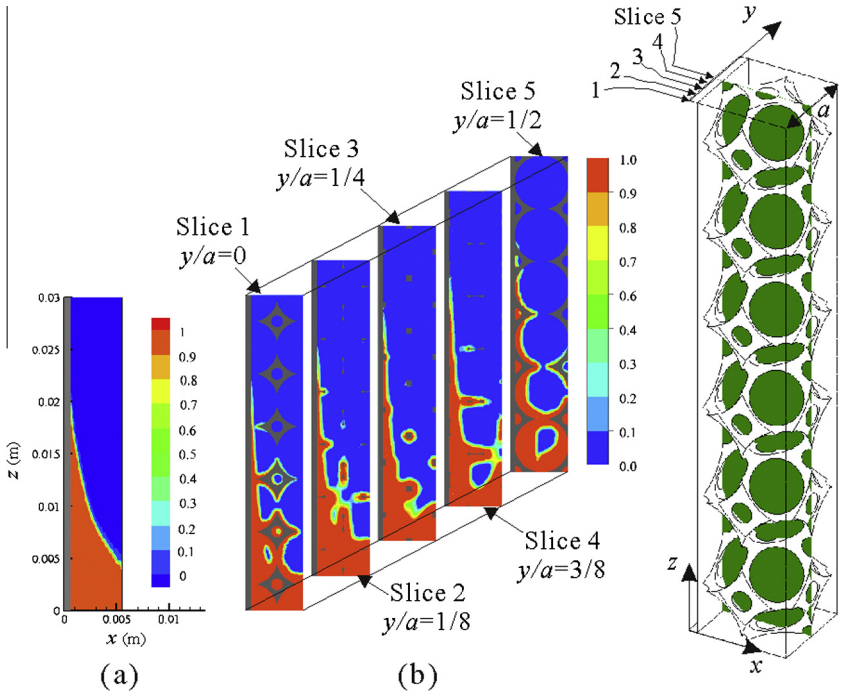

Fig. 6. Solid–liquid phase distributions predicted by (a) volume-averaged and (b) pore-scale simulation methods; with melt fraction = 0.25, corresponding to t = 30 s.

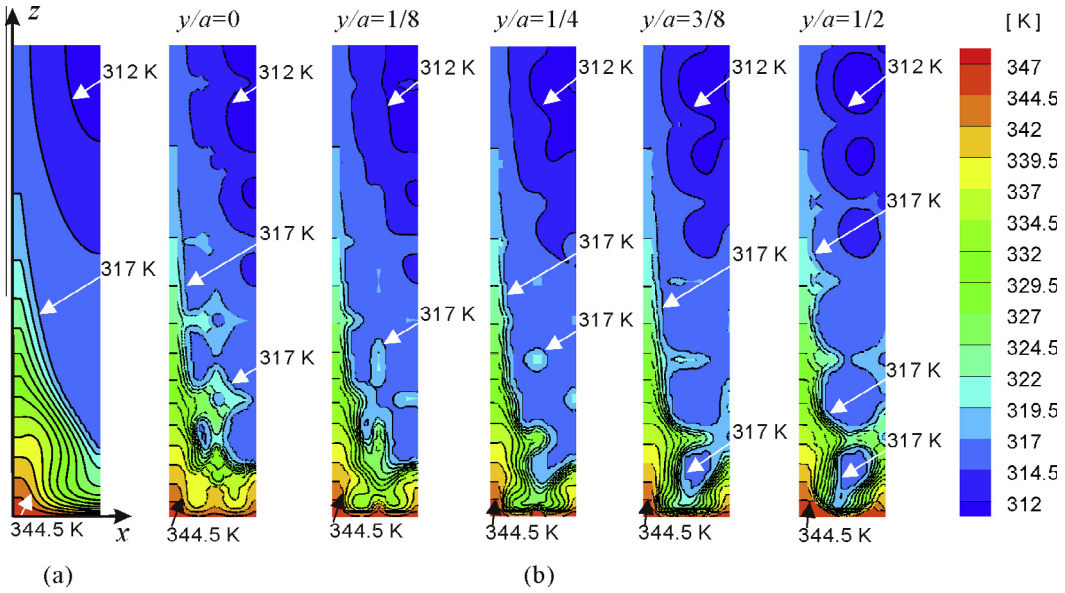

Fig. 7. Temperature distributions predicted by (a) volume-averaged and (b) pore-scale simulation methods, with melt fraction = 0.25, corresponding to t = 30 s; for pore-scale simulation, five slices are selected as shown in Fig. 6(b).

temperature moves downward, leading to global circulation of the liquid PCM. As shown in Fig. 8, the two simulation methods predict qualitatively similar flow circulation structures, and quantitatively the same maximum flow velocity (~0.004 m/s) at the channel center.

4.1.2. Melt fraction and surface heat flux

Once qualitative agreement between the two simulation methods is observed, a quantitative comparison is desired. Fig. 9 (a) and (b) compares the prediction results by the two simulation methods for evolution of volume fraction (i.e., melt fraction) of liquid PCM and bottom surface heat flux varying with the melting time, respectively. As significant natural convection is observed for the liquid PCM (referring to Fig. 8), it is therefore of interest to examine as well the contribution of natural convection on heat transfer. To this end results for with and without considering natural convection in the liquid PCM are both included in Fig. 9 (a) and (b).

The volume-averaged method with the one-temperature model is built upon the major assumption of local thermal equilibrium. While the pore-scale simulation considers the intricate foam geometry and couples the heat transfer between the metal foam

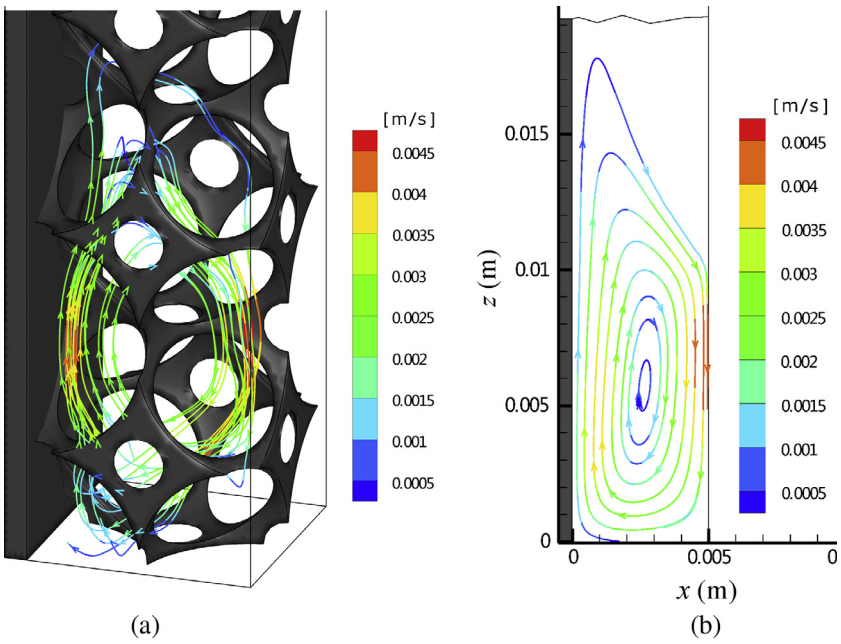

Fig. 8. Flow streamlines predicted by (a) pore-scale and (b) volume-averaged simulation methods, with melt fraction = 0.5 (t = 60 s).

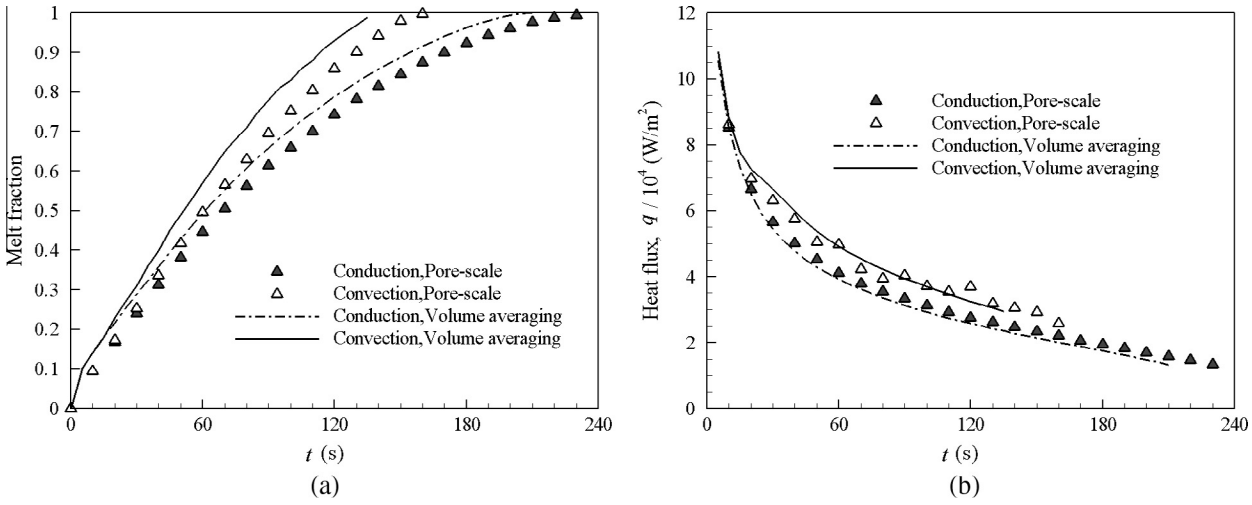

Fig. 9. Evolution of (a) volume fraction of liquid PCM and (b) bottom surface heat flux with time.

and the PCM, without needing the assumption of local thermal equilibrium. Therefore, the pore-scale simulation may be used as benchmark to check the applicability of the volume-averaged method with the one-temperature model. As shown in Fig. 9, reasonable agreements between the volume-averaged method with one-temperature model and the pore-scale method are observed, in terms of both melt fraction (Fig. 9(a)) and surface heat flux (Fig. 9(b)). Literature studies frequently applied the two-temperature model (in the volume-averaged simulation) to consider the heat transfer of metal foams with PCMs [13–16]. However, the interstitial heat transfer coefficients which are necessary in the two-temperature model are difficult to determine accurately, particularly at present there is no available models for the interstitial heat transfer between the metal foam and the static PCM (such as solid PCM or liquid PCM without motion). Further, the implementation of the two-temperature model is more difficult than the one-temperature model, especially if one should tackle with the heat flux continuity boundary condition between metal foam and a solid wall [10,29]. In comparison, the one-temperature model needs no interstitial heat transfer coefficients for closure and it is easier to implement numerically. The finding from Fig. 9 is significant because it indicates that the currently widely used, more complex two-temperature model is not necessary for paraffin infiltrated in metal foam. Although the present study only considered a single case, we believe that the exercise is still valuable and can shed light on the selection of one or two-temperature model for modeling metal foam and PCM system.

Literature studies demonstrated that the local thermal equilibrium or non-equilibrium conditions depend on the conductivity ratio and interstitial heat transfer between the two phases of a porous medium. Local thermal equilibrium condition is more likely to reach when the thermal conductivities of the two phases are closer [30] and the interstitial heat transfer is stronger [14]. It has been demonstrated that, for air forced convection in metal foams, the local thermal non-equilibrium prevails [31]. This may be attributed to the low thermal conductivity of air (~0.026 W/mK) relative to

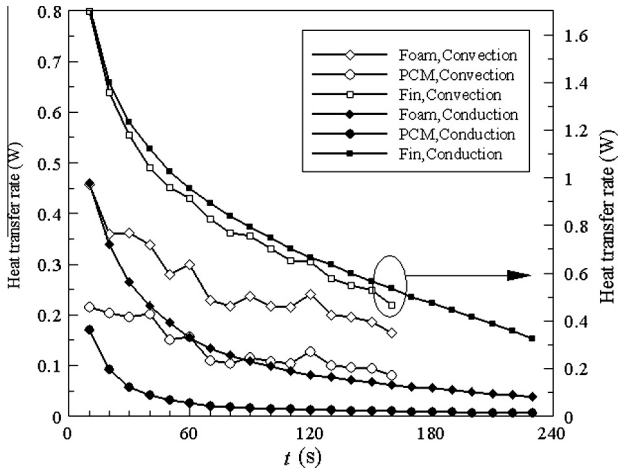

Fig. 10. Individual heat transfer rates from the bottom surface to fin, metal foam, and PCM: effect of natural convection on each of the three components.

that of metal and the low interstitial heat exchanging ability of air. However, if the cooling medium is replaced with water, Hunt and Tien [32] demonstrated that the one-temperature model (local thermal equilibrium) is adequate for forced convection of water in aluminum/nickel/carbon foams. Only few studies [17,26] have investigated the local thermal equilibrium between metal foam and PCMs. Through measuring the individual temperatures of copper foam and water (as PCM), Feng et al. [26] showed that thermal equilibrium holds between copper foam and water during freezing without natural convection. The simulation results of Hu and Patnalk [17] also indicated the local thermal equilibrium between metal foam and paraffin without natural convection. The present simulation results (in Fig. 9) further indicated the local thermal equilibrium between metal foam and paraffin with natural convection in liquid PCM.

Fig. 9 further shows that, the natural convection of liquid PCM plays a significant role on the melting heat transfer rate of PCM. For example, if natural convection is considered the total melting time is reduced by 28% compared to the case without considering the natural convection, and the bottom surface heat flux is increased by 10–25%. Note that the bottom surface heat flux given in Fig. 9(b) includes three terms: heat transfer from the bottom surface to the fin, metal foam, and PCM. To separate the effect of natural convection on each of the three terms, Fig. 10 presents the individual heat transfer rates from the bottom surface to the fin, metal foam and PCM, for two different conditions: with and without considering the natural convection. These heat transfer rates are pore-scale simulation results. It should be pointed out that the left and right side of the graph refer to the same parameter, but with different scale bars to show better each curve in the graph.

As shown in Fig. 10, natural convection significantly increases the heat transfer from the bottom surface to the PCM and metal foam. The reason is explained as follow. In the absence of natural convection, the heat transfer from the bottom surface to the PCM is through purely heat conduction, which is negligibly small (except during the initial stage of melting) due to the low thermal conductivity of PCM. However, if natural convection is considered, the cold liquid PCM at the channel center flows downward and then impinges onto the bottom surface (referring to Fig. 8), which increases the heat transfer from the bottom surface to the PCM significantly. On the other hand, the natural convection of liquid PCM promotes interstitial heat exchange between the foam matrix and the PCM, which ultimately increases the heat transfer rate from the bottom surface to the foam. When natural convection is considered, the heat transfer from the bottom surface to the fin is slightly decreased, this may be attributed to the fact that the vertical fin is in contact with the hot fluid stream that moves upward along the fin surface.

4.2. Thermal performance comparison among finned metal foam, plate-fin and metal foam

In this section, the thermal performance of the proposed finned metal foam is compared with the conventional plate-fin and metal foam without fin insertions. The plate-fin and metal foam considered in the comparison have the same geometrical dimensions (e.g., fin thickness and pitch, foam porosity, etc) as those of the finned metal foam. Evolution of the melt fraction predicted by the pore-scale method for the three structures is compared in Fig. 11(a). The melting rate is reflected by the slope of the melt fraction versus melting time curve, as shown in Fig. 11(a), the finned metal foam yields the highest melting rate among the three structures. The melting rate of the metal foam decreases continuously with time, this is because the convection of liquid PCM in metal foam is weak and the main heat transfer is through conduction, as the liquid PCM layer becomes thicker, the conduction

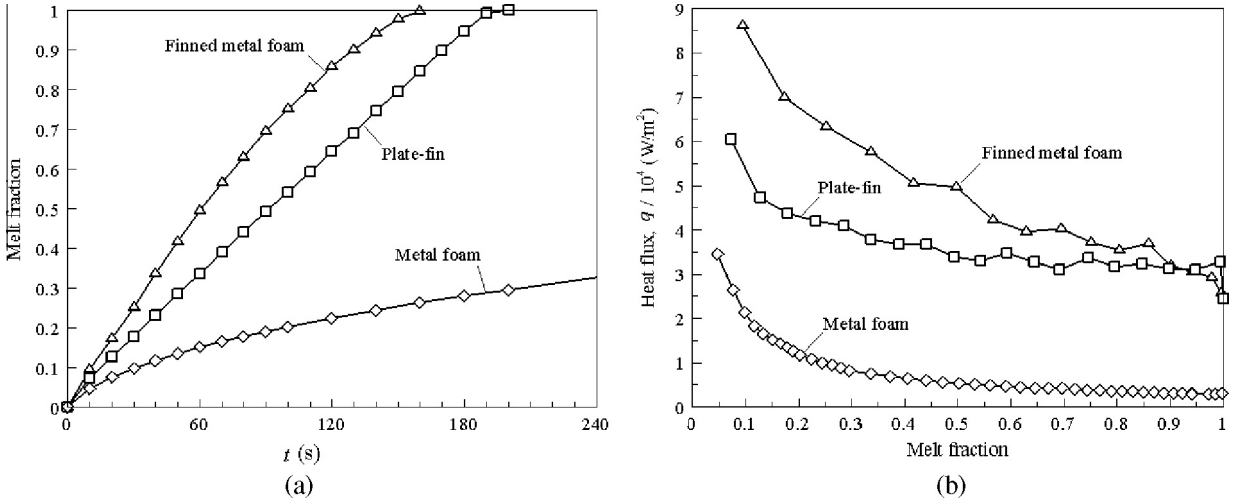

Fig. 11. Comparison among finned metal foam, plate-fin, and metal foam: (a) melt fraction plotted as a function of time; (b) bottom surface heat flux plotted as a function of melt fraction.

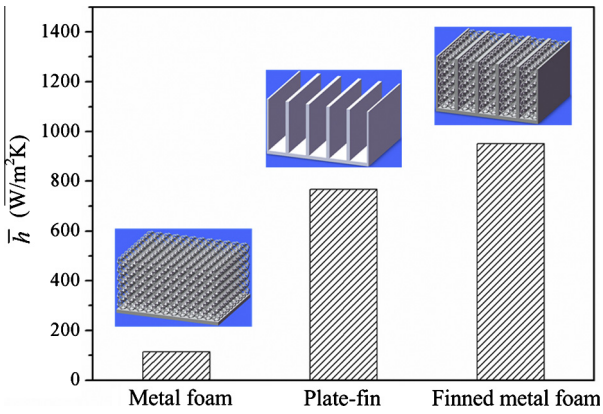

Fig. 12. Comparison of average heat transfer coefficients among the three competing structures for latent heat storage.

resistance in the liquid PCM layer increases and therefore the melting rate decreases as the melting process continues. However, for the conventional plate-fin structure, the open channel between adjacent fins allows predominant natural convection of the liquid PCM, which promotes the heat transfer from the fin and bottom surface to the phase front. As a result, the melting rate of the plate-fin is constant during the melting process.

Fig. 11(b) compares the bottom surface heat flux of the three structures plotted as a function of the melt fraction. For all the three structures, at initial state (small melt fraction) the surface heat flux is high, as the melt fraction increases the heat flux decreases under a constant temperature boundary condition. Relative to the plate-fin structure, inserting a metal foam block into the fin-channel is twofold: promoting heat conduction in the PCM and suppressing natural convection of the liquid PCM. When the melt fraction is small, convection in liquid PCM is weak and conduction is more important. Correspondingly, the heat flux of the finned metal foam is significantly higher than that of the plate-fin, due to the heat conduction enhancement by the metal foam. However, as the melt fraction increases, heat convection of liquid PCM in plate-fin becomes stronger than that in the finned metal foam. As a result, the heat flux of plate-fin approaches to that of the finned metal foam gradually as increasing the melting fraction, as shown in Fig. 11(b).

To facilitate quantitative comparison of the thermal performance, a heat transfer coefficient averaged over the entire melting process is introduced, as:

$$\bar{h} = \frac{\int_0^{\Delta t} q dt}{\Delta t \cdot \Delta T} \tag{19}$$

where q is the bottom surface heat flux varying with the melting time, Δt is the time required to complete the melting process, ΔT ($=T_w - T_0$) is the temperature difference between the bottom surface and the initial temperature. The average heat transfer coefficients of the three structures are calculated and shown in Fig. 12. The average heat transfer coefficient of the finned metal foam is 24% higher than that of the plate-fin, and about 7 times higher than that of the metal foam. The average heat transfer coefficients are proportional to the volume fraction of conductive solid introduced into the PCM for a given storing volume, which are 3%, 9.1%, and 11.8% for metal foam, plate-fin, and finned metal foam, respectively. Note that in the comparison the contact resistance between foam blocks and solid fins which may influence the performance of finned metal foam is not considered. According to our previous experience in Ref. [10] for forced air convection in finned metal foam, if the metal foam blocks are bonded to the solid fins properly through sintering or high thermal conductivity adhesive, the influence of contact resistance is negligible. Furthermore, in Ref. [26] the authors experimentally tested the effect of contact resistance for freezing of water infiltrated in metal foams. Three contact conditions were considered, i.e., natural contact, applied pressure, and bonding with a high thermal conductivity adhesive. It was found that the effect of different contact conditions on freezing rate is negligible within the range of experimental uncertainty.

5. Conclusions

A case study for melting of paraffin infiltrated in a finned metal foam was investigated using volume-averaged and pore-scale numerical simulation methods. The volume-averaged method employed the one-temperature model based on the local thermal equilibrium assumption. The pore-scale simulation method considered the intricate foam geometry and was free from the local thermal equilibrium assumption. Qualitatively, the two simulation methods led to similar predictions for the solid–liquid phase, temperature, and velocity distributions. Quantitatively, good agreements were achieved between the two methods in terms of melt fraction and surface heat flux. The case study demonstrated that the volume-averaged method with one-temperature model is applicable to consider paraffin infiltrated metal foam. The effect of natural convection in liquid PCM was explored. It was found that the melting process was expedited by the global natural convection of liquid PCM: for the simulation example investigated, the total melting time was reduced by 28% and the surface heat flux was increased by 10–25% relative to the case without considering natural convection. Compared with competing structures such as convectional plate-fin and metal foam, the proposed finned metal foam exhibited superior thermal performance, showing its great potential in latent heat storage applications.

Conflict of interest

None declared.

Acknowledgments

This work was supported by the National Natural Science Foundation of China (51206128), the National Basic Research Program of China (2011CB610305), the National "111" Project of China (B06024), the Postdoctoral Science Foundation of China (2012M521766), the Shaanxi Province Science Foundation and the Fundamental Research Funds for the Central Universities of China.

References

[1] N. Amin, M. Belusko, F. Bruno, An effectiveness-NTU model of a packed bed PCM thermal storage system, Appl. Energy 134 (2014) 356–362.
[2] N. Amin, F. Bruno, M. Belusko, Effective thermal conductivity for melting in PCM encapsulated in a sphere, Appl. Energy 122 (2014) 280–287.
[3] N. Amin, F. Bruno, M. Belusko, Effectiveness–NTU correlation for low temperature PCM encapsulated in spheres, Appl. Energy 93 (2012) 549–555.
[4] N. Amin, M. Belusko, F. Bruno, et al., Optimising PCM thermal storage systems for maximum energy storage effectiveness, Sol. Energy 86 (9) (2012) 2263–2272.
[5] K. Lafdi, O. Mesalhy, S. Shaikh, Experimental study on the influence of foam porosity and pore size on the melting of phase change materials, J. Appl. Phys. 102 (2007).
[6] C.Y. Zhao, W. Lu, Y. Tian, Heat transfer enhancement for thermal energy storage using metal foams embedded within phase change materials (PCMs), Sol. Energy 84 (2010) 1402–1412.
[7] D. Fernandes, F. Pitié, G. Cáceres, J. Baeyens, Thermal energy storage: "how previous findings determine current research priorities", Energy 39 (2012) 246–257.
[8] A. Bhattacharya, R.L. Mahajan, Finned metal foam heat sinks for electronics cooling in forced convection, J. Electron. Packag. 124 (2002) 155–163.
[9] A. Bhattacharya, R.L. Mahajan, Metal foam and finned metal foam heat sinks for electronics cooling in buoyancy-induced convection, J. Electron. Packag. 128 (2006) 259–266.

[10] S.S. Feng, J.J. Kuang, T. Wen, T.J. Lu, K. Ichimiya, An experimental and numerical study of finned metal foam heat sinks under impinging air jet cooling, Int. J. Heat Mass Transfer 77 (2014) 1063–1074.
[11] C. Beckermann, R. Viskanta, Natural convection solid/liquid phase change in porous media, Int. J. Heat Mass Transfer 31 (1) (1988) 35–46.
[12] K.T. Harris, A. Haji-Sheikh, A.A. Nnanna, Phase-change phenomena in porous media–a non-local thermal equilibrium model, Int. J. Heat Mass Transfer 44 (8) (2001) 1619–1625.
[13] O. Mesalhy, K. Lafdi, A. Elgafy, K. Bowman, Numerical study for enhancing the thermal conductivity of phase change material (PCM) storage using high thermal conductivity porous matrix, Energy Convers. Manage. 46 (2005) 847–867.
[14] S. Krishnan, J.Y. Murthy, S.V. Garimella, A two-temperature model for solid–liquid phase change in metal foams, J. Heat Transfer 127 (2005) 995–1004.
[15] Y. Tian, C.Y. Zhao, A numerical investigation of heat transfer in phase change materials (PCMs) embedded in porous metals, Energy 36 (2011) 5539–5546.
[16] W.Q. Li, Z.G. Qu, Y.L. He, W.Q. Tao, Experimental and numerical studies on melting phase change heat transfer in open-cell metallic foams filled with paraffin, Appl. Therm. Eng. 37 (2012) 1–9.
[17] X. Hu, S.S. Patnaik, Modeling phase change material in micro-foam under constant temperature condition, Int. J. Heat Mass Transfer 68 (2014) 677–682.
[18] S.S. Sundarram, W. Li, The effect of pore size and porosity on thermal management performance of phase change material infiltrated microcellular metal foams, Appl. Therm. Eng. 64 (2014) 147–154.
[19] Z. Chen, D. Gao, J. Shi, Experimental and numerical study on melting of phase change materials in metal foams at pore scale, Int. J. Heat Mass Transfer 72 (2014) 646–655.
[20] A.J. Queimada, S.E. Quinones-Cisneros, I.M. Marrucho, J.A.P. Coutinho, E.H. Stenby, Viscosity and liquid density of asymmetric hydrocarbon mixtures, Int. J. Thermophys. 24 (2003) 1221–1239.
[21] M. Bai, J.N. Chung, Analytical and numerical prediction of heat transfer and pressure drop in open-cell metal foams, Int. J. Therm. Sci. 50 (2011) 869–880.
[22] ANSYS Fluent Software Package: User's Manual, Version 14, 2011.
[23] V.V. Calmidi, Transport phenomena in high porosity fibrous metal foams (Ph.D. thesis), University of Colorado, 1998.
[24] A. Bhattacharya, V.V. Calmidi, R.L. Mahajan, Thermophysical properties of high porosity metal foams, Int. J. Heat Mass Transfer 45 (2002) 1017–1031.
[25] S. Krishnan, J.Y. Murthy, S.V. Garimella, Direct simulation of transport in open-cell metal foam, J. Heat Transfer 128 (2006) 793–799.
[26] S.S. Feng, Y. Zhang, M. Shi, T. Wen, T.J. Lu, Unidirectional freezing of phase change materials saturated in open-cell metal foams, Appl. Therm. Eng. (2014), http://dx.doi.org/10.1016/j.applthermaleng.2014.09.055.
[27] S.S. Feng, T. Kim, T.J. Lu, Numerical investigation of forced convection in pin/plate-fin heat sinks heated by impinging jet using porous medium approach, Int. J. Numer. Meth. Heat Fluid Flow 23 (1) (1991) 88–107.
[28] S. Patankar, Numerical Heat Transfer and Fluid Flow, McGraw-Hill, NY, 1980.
[29] C.T. DeGroot, A.G. Straatman, L.J. Betchen, Modeling forced convection in finned metal foam heat sinks, J. Electron. Packag. 131 (2) (2009) 021001.
[30] D.Y. Lee, K. Vafai, Analytical characterization and conceptual assessment of solid and fluid temperature differentials in porous media, Int. J. Heat Mass Transfer 42 (3) (1999) 423–435.
[31] V. Calmidi, R. Mahajan, Forced convection in high porosity metal foams, J. Heat Transfer 122 (3) (2000) 557–565.
[32] M.L. Hunt, C.L. Tien, Effects of thermal dispersion on forced convection in fibrous media, Int. J. Heat Mass Transfer 31 (1988) 301–309.